Measurement of the charge asymmetry for the $K_S \to \pi e \nu$ decay and test of CPT symmetry with the KLOE detector

The KLOE-2 Collaboration

A. Anastasi[a,b] **D. Babusci**[b] **M. Berłowski**[b,c] **C. Bloise**[b] **F. Bossi**[b] **P. Branchini**[d]
A. Budano[e,d] **B. Cao**[f] **F. Ceradini**[e,d] **P. Ciambrone**[b] **G. Capon**[b] **F. Curciarello**[b]
E. Czerwiński[g] **G. D'Agostini**[h,i] **E. Danè**[b] **V. De Leo**[k] **E. De Lucia**[b] **A. De Santis**[b]
P. De Simone[b] **A. Di Cicco**[e,d] **A. Di Domenico**[h,i] **D. Domenici**[b] **A. D'Uffizi**[b]
A. Fantini[l,k] **G. Fantini**[m] **P. Fermani**[b] **S. Fiore**[n,i] **A. Gajos**[g] **P. Gauzzi**[h,i] **S. Giovannella**[b]
E. Graziani[d] **V. L. Ivanov**[o,r] **T. Johansson**[f] **X. Kang**[b] **D. Kisielewska-Kamińska**[g]
E. A. Kozyrev[o,r] **W. Krzemień**[c] **A. Kupść**[f] **S. Loffredo**[e,d] **P. A. Lukin**[o,r]
G. Mandaglio[p,s] **M. Martini**[b,j] **R. Messi**[l,k] **S. Miscetti**[b] **D. Moricciani**[k] **P. Moskal**[g]
A. Passeri[d] **V. Patera**[t,i] **E. Perez del Rio**[b] **N. Raha**[k] **P. Santangelo**[b] **M. Schioppa**[v,w]
A. Selce[e,d] **M. Silarski**[g] **F. Sirghi**[b,x] **E. P. Solodov**[o,r] **L. Tortora**[d] **G. Venanzoni**[y]
W. Wiślicki[c] **M. Wolke**[f]

[a]*Dipartimento di Scienze Matematiche e Informatiche, Scienze Fisiche e Scienze della Terra dell'Università di Messina, Messina, Italy.*

[b]*Laboratori Nazionali di Frascati dell'INFN, Frascati, Italy.*

[c]*National Centre for Nuclear Research, Warsaw, Poland.*

[d]*INFN Sezione di Roma Tre, Roma, Italy.*

[e]*Dipartimento di Matematica e Fisica dell'Università "Roma Tre", Roma, Italy.*

[f]*Department of Physics and Astronomy, Uppsala University, Uppsala, Sweden.*

[g]*Institute of Physics, Jagiellonian University, Cracow, Poland.*

[h]*Dipartimento di Fisica dell'Università "Sapienza", Roma, Italy.*

[i]*INFN Sezione di Roma, Roma, Italy.*

[j]*Dipartimento di Scienze e Tecnologie applicate, Università "Guglielmo Marconi", Roma, Italy.*

[k]*INFN Sezione di Roma Tor Vergata, Roma, Italy.*

[l]*Dipartimento di Fisica dell'Università "Tor Vergata", Roma, Italy.*

[m]*Gran Sasso Science Institute, L'Aquila, Italy.*

[n]*ENEA UTTMAT-IRR, Casaccia R.C., Roma, Italy*

[o]*Budker Institute of Nuclear Physics, Novosibirsk, Russia.*

[p]*Dipartimento di Scienze Chimiche, Biologiche, Farmaceutiche ed Ambientali dell'Università di Messina, Messina, Italy.*

[r]*Novosibirsk State University, Novosibirsk, Russia.*

[s]*INFN Sezione di Catania, Catania, Italy.*

^{t}*Dipartimento di Scienze di Base ed Applicate per l'Ingegneria dell'Università "Sapienza", Roma, Italy.*

^{u}*INFN Sezione di Bari, Bari, Italy.*

^{v}*Dipartimento di Fisica dell'Università della Calabria, Rende, Italy.*

^{w}*INFN Gruppo collegato di Cosenza, Rende, Italy.*

^{x}*Horia Hulubei National Institute of Physics and Nuclear Engineering, Măgurele, Romania*

^{y}*INFN Sezione di Pisa, Pisa, Italy.*

ABSTRACT: Using 1.63 fb^{-1} of integrated luminosity collected by the KLOE experiment about 7×10^4 $K_S \to \pi^\pm e^\mp \nu$ decays have been reconstructed. The measured value of the charge asymmetry for this decay is $A_S = (-4.9 \pm 5.7_{stat} \pm 2.6_{syst}) \times 10^{-3}$, which is almost twice more precise than the previous KLOE result. The combination of these two measurements gives $A_S = (-3.8 \pm 5.0_{stat} \pm 2.6_{syst}) \times 10^{-3}$ and, together with the asymmetry of the K_L semileptonic decay, provides significant tests of the CPT symmetry. The obtained results are in agreement with CPT invariance.

Contents

1 Introduction

Semileptonic decays have been of fundamental importance in establishing several properties of the neutral kaon system, and of the Standard Model in general, including the $\Delta S = \Delta Q$ rule [1], CP violation [2], and the unitarity of the quark mixing matrix [3, 4].

The asymmetries which can be constructed from the decay rates into the two CP conjugated semileptonic final states, $\pi^- e^+ \nu$ and $\pi^+ e^- \bar{\nu}$, constitute a powerful probe in the study of discrete symmetries [5]. In particular, the charge asymmetries for the physical states K_S and K_L defined as:

$$A_{S,L} = \frac{\Gamma(K_{S,L} \to \pi^- e^+ \nu) - \Gamma(K_{S,L} \to \pi^+ e^- \bar{\nu})}{\Gamma(K_{S,L} \to \pi^- e^+ \nu) + \Gamma(K_{S,L} \to \pi^+ e^- \bar{\nu})} \tag{1.1}$$

are sensitive to CP violation effects. At first order in small parameters [6]:

$$A_{S,L} = 2 \left[Re\left(\epsilon_K\right) \pm Re\left(\delta_K\right) - Re(y) \pm Re(x_-) \right] \tag{1.2}$$

with $Re\left(\epsilon_K\right)$ and $Re\left(\delta_K\right)$ implying T- and CPT-violation in the $K^0 - \overline{K^0}$ mixing, respectively, $Re(y)$ and $Re(x_-)$ implying CPT violation in $\Delta S = \Delta Q$ and $\Delta S \neq \Delta Q$ decay amplitudes, respectively[1], and all parameters implying CP violation. If CPT symmetry holds then the two asymmetries are expected to be identical $A_S = A_L = 2 \, Re\left(\epsilon_K\right) \simeq 3 \times 10^{-3}$ each accounting for the CP impurity in the mixing in the corresponding physical state.

The CPT theorem ensures exact CPT invariance for quantum field theories - like the Standard Model - formulated on flat space-time and assuming Lorentz invariance, locality, and hermiticity [7]. CPT violation effects might arise in a quantum gravity scenario [8, 9] and their observation would constitute an unambiguous signal of processes beyond the Standard Model.

In this context the measurement of the difference $A_S - A_L = 4 \left(Re\,\delta_K + Re\,x_- \right)$ is of particular importance as a test of the CPT symmetry. This observable is well constrained and can provide a test based on the direct comparison of a transition probability with its CPT conjugated transition - realised with entangled neutral kaon pairs - which constitutes one of the most precise, robust and model independent tests of the CPT symmetry [10].

The sum $A_S + A_L = 4 \left(Re\,\epsilon_K - Re\,y \right)$ can be used to extract the CPT-violating parameter $Re(y)$ once the measured value of $Re(\epsilon_K)$ is provided as input.

The two combinations $A_S \pm A_L$ (dominated by the uncertainty on A_S) constitute also a fundamental ingredient for improving the semileptonic decay contribution to the CPT test obtained imposing the unitarity relationship, originally derived by Bell and Steinberger [11], and yielding the most stringent limits on $Im(\delta)$ and the mass difference $m(K^0) - m(\overline{K^0})$ [12, 13].

---

[1]More explicitly y and x_- are described in terms of the decay amplitudes $\mathcal{A}_\pm = A(K^0 \to e^\pm \pi^\mp \nu(\bar{\nu}))$ and $\bar{\mathcal{A}}_\pm = A(\bar{K}^0 \to e^\pm \pi^\mp \nu(\bar{\nu}))$ as:

$$y = \frac{\bar{\mathcal{A}}_-^* - \mathcal{A}_+}{\bar{\mathcal{A}}_-^* + \mathcal{A}_+}, \quad x_- = \frac{1}{2} \left[\frac{\bar{\mathcal{A}}_+}{\mathcal{A}_+} - \left(\frac{\mathcal{A}_-}{\bar{\mathcal{A}}_-} \right)^* \right]. \tag{1.3}$$

At present, the most precise measurement of A_L has been performed by the KTeV collaboration: $A_L = (3.322 \pm 0.058_{stat} \pm 0.047_{syst}) \times 10^{-3}$ [14]. The measurement of its counterpart, A_S, requires a very pure K_S beam which can only be realised exploiting the entangled neutral kaons pairs produced at a ϕ-factory [15].

The first measurement of A_S has been performed by the KLOE collaboration using 410 pb^{-1} of integrated luminosity collected at DAΦNE [16], the ϕ-factory of the INFN laboratories of Frascati: $A_S = (1.5 \pm 9.6_{stat} \pm 2.9_{syst}) \times 10^{-3}$ [17], with an accuracy dominated by the statistical uncertainty. The new measurement reported here is based on a four times larger data sample, corresponding to an integrated luminosity of 1.63 fb^{-1}. The combination of the two results has a precision approaching the level of the CP violation effects expected for K_S under the assumption of CPT invariance. New limits on $Re(y)$ and $Re(x_-)$ have been also derived.

2 The KLOE detector

The KLOE detector operates at the DAΦNE electron-positron collider. The energy of the two colliding beams is set to the mass of the ϕ meson which decays predominantly into a pair of charged or neutral kaons. Since the beams cross at an angle of 2×12.5 mrad the ϕ-meson is produced with a small momentum of $p_\phi \approx 13$ MeV.

The KLOE detector consists of two main components: the cylindrical drift chamber and the electromagnetic calorimeter, both surrounding the beam pipe and immersed in a 0.52 T axial magnetic field. The drift chamber (DC) is a 3.3 m long cylinder with internal and external radii of 25 cm and 2 m, respectively. The chamber structure is made of carbon-fiber epoxy composite and the gas mixture used is 90% helium, 10% isobutane. These features maximize transparency to photons and reduce charged particle multiple scattering and $K_L \to K_S$ regeneration. About 40% of produced K_L mesons decay inside the DC volume, while most of the surviving K_L's interact and are detected in the electromagnetic calorimeter. Around 12500 sense wires stretched between the DC endplates allow to obtain a track spatial resolution of ~ 2 mm along the axis and better than 200 μm in the transverse plane. The accuracy on the decay vertex determination is ~ 1 mm and the resolution of the particle transverse momentum is 0.4 % [18]. The electromagnetic calorimeter (EMC) made by lead and scintillating fibers is divided into a barrel and two end-caps, has a readout granularity of $\sim (4.4 \times 4.4)$ cm^2, for a total of 2440 cells arranged in five layers covering 98% of the solid angle. It has energy and time resolution of $\sigma(E)/E = 5.7\%/\sqrt{E[\text{GeV}]}$, $\sigma_t = 54$ ps$/\sqrt{E[\text{GeV}]} \oplus 140$ ps for photons and electrons [19].

The data acquisition is enabled by a two-level trigger system [20]. The first level trigger is a fast trigger with a minimal delay which starts the acquisition at the front-end electronics. It requires two local energy deposits above threshold (50 MeV on the barrel, 150 MeV on the end-caps). The trigger time is determined by the first particle reaching the calorimeter and is synchronized with the DAΦNE RF signal.

The second level trigger uses information from both the drift chamber and the electromagnetic calorimeter. The trigger decision can be vetoed if the event is recognised as

Bhabha scattering or cosmic ray event. For control purposes these events are accepted and saved as dedicated downscaled samples.

The time interval between bunch crossings ($T_{bunch} = 2.715$ ns) is smaller than the time spread of the registered signals originating from $K_L K_S$ events that can reach 30-40 ns. The offline reconstruction procedure therefore has to determine the true bunch crossing time T_0 for each event and correct all times related to that event accordingly. In the reconstruction algorithm the T_0 is determined by using the EMC information. In the studied channel, since the K_S decay time is smaller than the K_L interaction time in the calorimeter, the T_0 time has to be corrected in the offline analysis.

The data sample used for this analysis has been processed and filtered with the KLOE standard reconstruction software and the event classification procedure. The simulated data samples are based on the Monte Carlo (MC) GEANFI program [21].

3 Measurement of $K_S \to \pi e \nu$ charge asymmetry

The charge asymmetry for the short-lived kaon is given by:

$$A_S = \frac{N^+/\epsilon^+ - N^-/\epsilon^-}{N^+/\epsilon^+ + N^-/\epsilon^-}, \tag{3.1}$$

where N^+ and N^- are the numbers of observed $K_S \to \pi^- e^+ \nu$ and $K_S \to \pi^+ e^- \bar{\nu}$ decays, respectively, while ϵ^+ and ϵ^- are the corresponding efficiencies. Negative and positive charged pions interact differently in the detector material, therefore the efficiency is separately estimated for $\pi^- e^+ \nu$ and $\pi^+ e^- \bar{\nu}$ final charge states.

3.1 K_S tagging

The interaction of a K_L meson in the calorimeter (crash) tags the presence of a K_S meson. K_L candidates must deposit an energy $E_{clu}(crash) > 100$ MeV in the calorimeter in the polar angle range $40° < \theta < 140°$ and not associated with a track from the DC. Since the kaon velocity in the ϕ meson rest frame is well-defined ($\beta^* \sim 0.22$), the requirement $0.18 < \beta^* < 0.27$ is applied. The K_L direction obtained from the K_L interaction coordinates in the calorimeter allows to determine the K_L momentum $\vec{p}_{K_L}$ with good precision, and hence the K_S momentum: $\vec{p}_{K_S} = \vec{p}_\phi - \vec{p}_{K_L}$.

3.2 Momenta smearing

In order to improve the MC simulation description of the experimental momentum resolution effects, the reconstructed MC track momentum components p_i have been smeared using three Gaussian functions:

$$p_i^{new} = p_i \times (1 + \alpha_p) \times (1 + \Delta \cdot \sum_{j=1}^{3} f_j \cdot G(0, \sigma_j)), \qquad (i = x, y, z) \tag{3.2}$$

where $G(0, \sigma_j)$ is the Gaussian distribution with zero mean and standard deviation σ_j, f_j is its amplitude, while Δ is the fractional uncertainty on the track curvature.

The momentum shift α_p and the Gaussian parameters are tuned on the $K_L \to \pi e\nu$ control sample (see Section 4). The fit yields $f_1 = 96\%$, $\sigma_1 = 0.34$, $f_2 = 3.2\%$, $\sigma_2 = 9.74$, $f_3 = 0.8\%$, $\sigma_3 = 71.2$ and $\alpha_p = 1.37 \cdot 10^{-4}$.

3.3 Event preselection

The selection of $K_S \to \pi e\nu$ decays starts with the reconstruction of a vertex formed by two opposite curvature tracks close to the e^+e^- interaction point (IP) with $\rho_{vtx} < 15$ cm and $|z_{vtx}| < 10$ cm, being ρ_{vtx} and z_{vtx} the transverse distance and the longitudinal coordinate of the vertex, respectively. In the majority of the three-body decays of K_S the angle between charged secondaries (α) is contained in the $(70°, 175°)$ range in the K_S rest frame, as shown in the left panel of Figure 1. Since the main source of background originates from the $K_S \to \pi^+\pi^-$ decay, a cut on the invariant mass under the assumption of both particles being charged pions is also applied (300 MeV $< M_{inv}(\pi, \pi) < 490$ MeV), as indicated in the right panel of Figure 1.
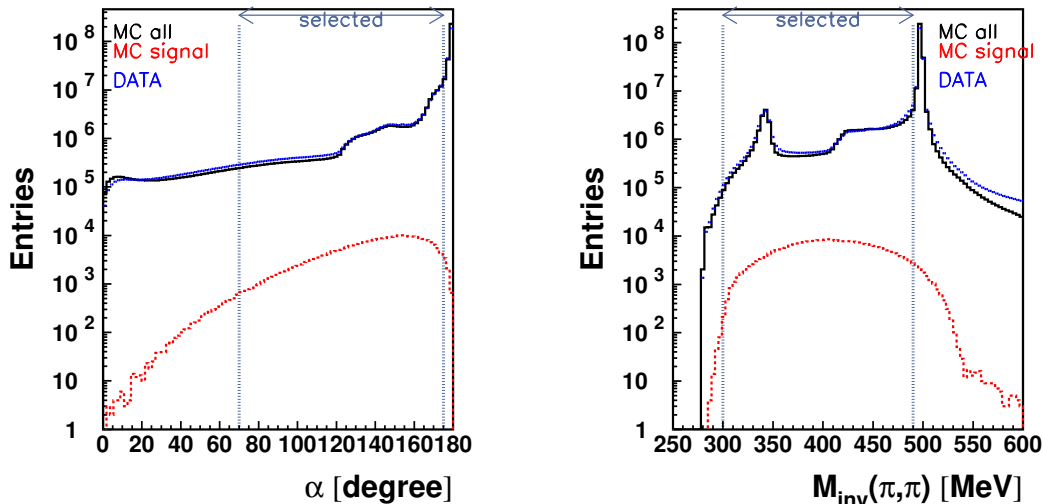

Figure 1. Left: Distribution of the α angle between charged secondaries in K_S rest frame. Right: Distribution of the invariant mass $M_{inv}(\pi, \pi)$ calculated under the assumption that both reconstructed tracks are pions. In both figures black solid lines represent all simulated events, the red dashed lines show simulated $K_S \to \pi e\nu$ signal events and blue points are data. Vertical dashed lines represent the cuts described in the text.

Both tracks reconstructed in the drift chamber must be associated with clusters in the calorimeter by the Track to Cluster Association (TCA) procedure. This procedure extrapolates each track from the last hit in the DC towards the calorimeter surface and determines the impact point.

3.4 Time of flight selection cuts

Further background reduction and final charged state ($\pi^\pm e^\mp$) identification is based on the difference $\delta_t(X)$ between the particle time of flight (TOF) from the K_S decay vertex to the

calorimeter $(t_{cl} - T_0)$, and the time calculated from the DC measurement of track length L and particle momentum p under the m_X mass hypothesis:

$$\delta_t(X) = (t_{cl} - T_0) - \frac{L}{c \cdot \beta(X)}, \quad \beta(X) = \frac{p}{\sqrt{p^2 + m_X^2}}. \tag{3.3}$$

Since at this stage the ϕ decay time (T_0) is not known with sufficient precision, the following difference is introduced:

$$\delta_t(X, Y) = \delta_t(X)_1 - \delta_t(Y)_2 , \tag{3.4}$$

where the mass hypothesis $m_{X(Y)}$ is used for track 1(2). Since for the correct mass assignments the value of $\delta_t(X, Y)$ is close to zero, the condition $|\delta_t(\pi, \pi)| > 1.5$ ns is applied for further $K_S \to \pi^+\pi^-$ rejection. The remaining pairs of tracks are tested under pion-electron $\delta_t(\pi, e)$ and electron-pion $\delta_t(e, \pi)$ hypothesis (see Figure 2). Once particle identification has been performed, the T_0 and the time differences $\delta_t(e)$ and $\delta_t(\pi)$ are reevaluated accordingly. Events are then selected within the circle in the $\delta_t(e) - \delta_t(\pi)$ plane as shown in Figure 3.
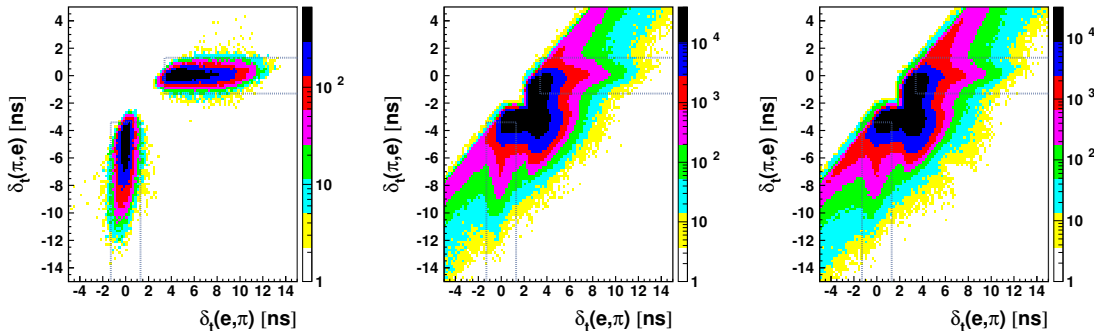

Figure 2. Distribution of TOF differences $\delta_t(\pi, e)$ vs $\delta_t(e, \pi)$ for simulated $K_S \to \pi e\nu$ events (left plot), all simulated events (center plot) and data (right plot). The signal events are selected in the regions delimited by the dashed lines: $(|\delta_t(e, \pi)| < 1.3$ ns, $\delta_t(\pi, e) < -3.4$ ns$)$ or $(\delta_t(e, \pi) > 3.4$ ns, $|\delta_t(\pi, e)| < 1.3$ ns$)$.

The best separation between the signal and background components is obtained with the variable:

$$M^2(e) = [E_{K_S} - E(\pi) - E_\nu]^2 - p^2(e), \tag{3.5}$$

where $E_\nu = |\vec{p}_{K_S} - \vec{p}(e) - \vec{p}(\pi)|$. $M^2(e)$ is calculated according to the TOF particle identification. For the signal events $M^2(e)$ peaks close to zero (see Figure 4).

3.5 Signal extraction

The signal yield is obtained by fitting the $M^2(e)$ distribution with a superposition of the corresponding simulated distributions for signal and residual background components, with free normalizations, separately for each final charge state, and taking into account the statistical uncertainty of the Monte Carlo sample [22, 23]. The remaining residual background components are:
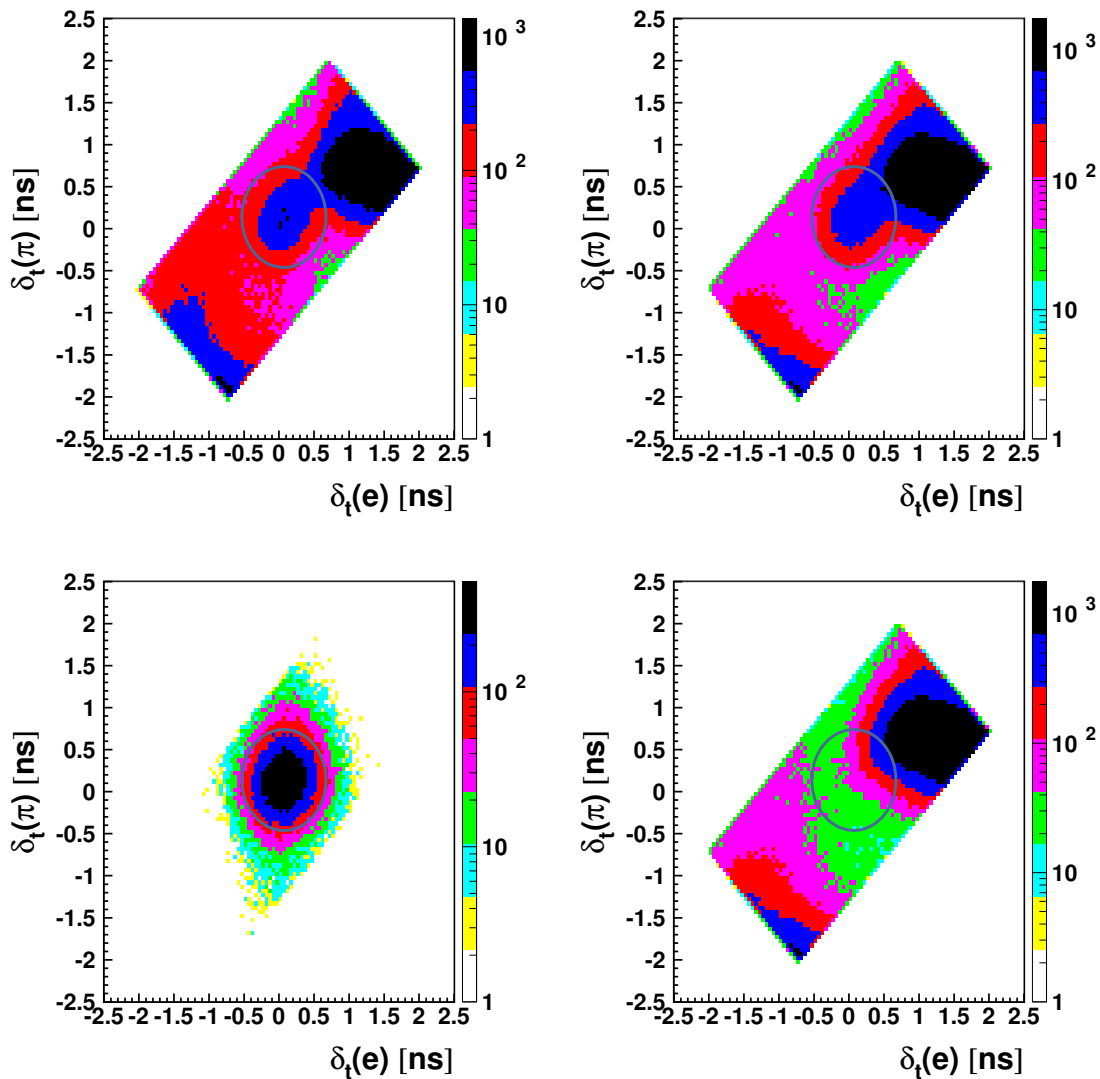
Figure 3. Distribution of the time differences $\delta_t(\pi)$ vs $\delta_t(e)$ for data events (top-left), all simulated events (top-right), simulated $K_S \to \pi e \nu$ events (bottom-left) and simulated background events (bottom-right). Events within the circle $[(\delta_t(e) - 0.07 \text{ ns})]^2 + [(\delta_t(\pi) - 0.13 \text{ ns})]^2 = (0.6 \text{ ns})^2$ are retained for the analysis.

- the $K_S \to \pi^+\pi^-$ decays with one of the pion tracks not correctly reconstructed and classified as an electron by the TOF algorithm (1.6% of the sample after the fit, summing on the two final charge states);

- the $K_S \to \pi^+\pi^-$ decays where one of the pions decays into a muon before entering the drift chamber (18.7%);

- radiative $K_S \to \pi^+\pi^-\gamma$ decays (2.5%);

- other decays mainly originating from $\phi \to K^+K^-$ (6.7%) .

The result of the fit for the signal events is 34579 ± 251 for $K_S \to \pi^- e^+ \nu$ and 36874 ± 255 for $K_S \to \pi^+ e^- \bar{\nu}$, with total $\chi^2/ndof = 118/109$, summing on the two final charge states (see Figure 4).
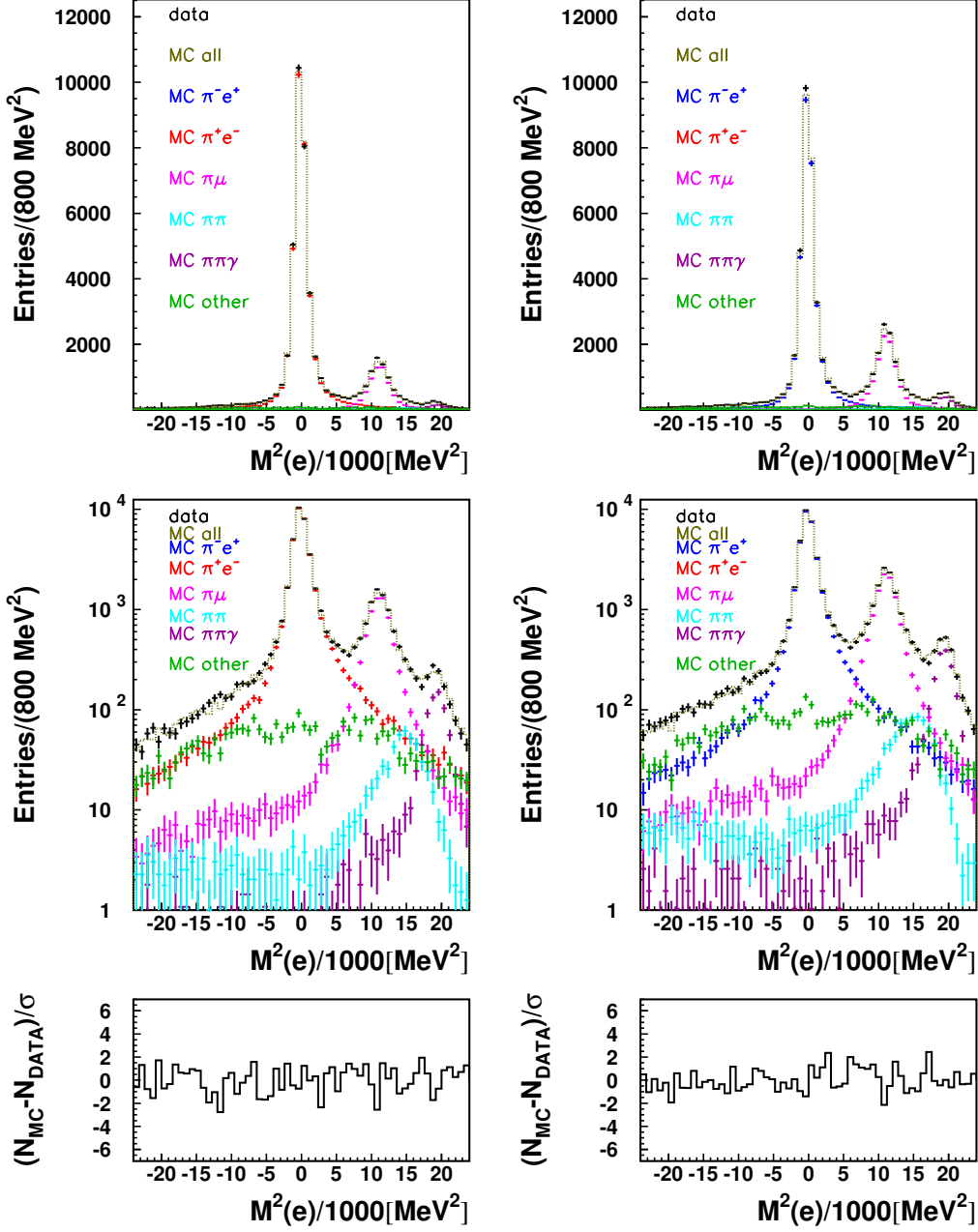

Figure 4. $M^2(e)$ distribution for data (black points) and MC simulation (dotted histogram) for both final charge states ($\pi^+ e^-$ – left side, $\pi^- e^+$ – right side) after the fit. The individual MC contributions are shown superimposed in the plots (colored points – see legend in the plots). Bottom row: corresponding data-MC residual distributions after the fit.

4 $K_L \to \pi e \nu$ control sample selection

A data sample of $K_L \to \pi e \nu$ decay, which is a dominant decay mode of K_L meson, is selected and used as a control sample. These events are tagged by the $K_S \to \pi^0 \pi^0$ decay[2], identified by a total energy deposition in the calorimeter greater than 300 MeV, single photon deposit in the range from 20 to 300 MeV, and the $\pi^0 \pi^0$ invariant mass in the range from 390 to 600 MeV. The estimated tag efficiency is $(60.0 \pm 0.3)\%$. No appreciable contamination is found from other ϕ meson decays and the beam-induced background is kept at the level of 1%.

Due to the different lifetimes of K_S and K_L, the vertex distribution of K_L decays is weighted to reproduce the K_S distribution. The weighting is performed bin-by-bin in the same $\rho_{vtx} - z_{vtx}$ acceptance region of the signal $K_S \to \pi e \nu$. In this way the $K_L \to \pi e \nu$ selected sample accurately mimics the signal.

The events of the control sample are used to estimate directly from data the efficiencies for positive and negative pions. To this aim a single track selection scheme is developed and applied, after vertex reconstruction and cuts on opening angle in K_L rest frame and $M_{inv}(\pi, \pi)$, as described in Section 3.3.

At this stage we require that at least one track reaches the calorimeter with TCA. For this track the $\delta_t(e)$ and $\delta_t(\pi)$ variables are constructed (see Equation 3.3). A pure sample of electrons (positrons) is then selected by requiring $[(\delta_t(e) - 0.07 \text{ ns})/1.2 \text{ ns}]^2 + [(\delta_t(\pi) + 4 \text{ ns})/3.2 \text{ ns}]^2 < 1$.

As the aforementioned procedure does not require extrapolation of the pion tracks towards the calorimeter, the selected sample is used for TCA and TOF efficiency evaluation separately for negative and positive pions.

5 Efficiency determination

The efficiency is estimated as follows:

$$\epsilon = \epsilon_{TEC} \cdot \epsilon_{TAG} \cdot \epsilon_{ANA}, \tag{5.1}$$

where ϵ_{TEC} stands for trigger and event classification efficiency, while ϵ_{TAG} and ϵ_{ANA} denote tagging and analysis efficiencies, respectively.

The analysis efficiency ϵ_{ANA} can be expressed in turn as a product of four contributions:

- kinematical cuts (ϵ_{KC}): cuts on reconstructed vertex fiducial volume, opening angle α, and $M_{inv}(\pi, \pi)$ (see Section 3.3);

- Track to Cluster Association algorithm (ϵ_{TCA});

- Time of Flight cuts (ϵ_{TOF});

- fit range (ϵ_{FR}) of the $M^2(e)$ variable.

---

[2] Quantum interference effects in the double decay $K_L K_S \to \pi e \nu, \pi^0 \pi^0$ are negligible in this specific case.

The efficiency ϵ_{TEC} is evaluated using downscaled minimum-bias data samples without event classification and background rejection filters. The estimation of ϵ_{TAG}, ϵ_{KC} and ϵ_{FR} are based on MC simulation. ϵ_{TCA} and ϵ_{TOF} are determined using the $K_L \to \pi e \nu$ control sample with the method described in Section 4. ϵ_{TCA} consists of the product of $\epsilon_{TCA}(\pi^{\pm})$ and $\epsilon_{TCA}(e^{\mp})$, corrected for the control sample derived efficiencies and using the MC efficiencies:

$$\epsilon_{TCA} = \epsilon_{TCA}^{KS}(\pi) \times \epsilon_{TCA}^{KS}(e) = \epsilon_{TCA}^{KL\,DATA}(\pi) \times \frac{\epsilon_{TCA}^{KS\,MC}(\pi)}{\epsilon_{TCA}^{KL\,MC}(\pi)} \times \epsilon_{TCA}^{KS\,MC}(e). \tag{5.2}$$

Then, the Time of Flight efficiency is determined using the $K_L \to \pi e \nu$ data control sample in a similar manner:

$$\epsilon_{TOF}^{KS} = \epsilon_{TOF}^{KL\,DATA} \times \frac{\epsilon_{TOF}^{KS\,MC}}{\epsilon_{TOF}^{KL\,MC}}. \tag{5.3}$$

The total efficiency is $(7.39 \pm 0.03)\%$ and $(7.81 \pm 0.03)\%$, for $K_S \to \pi^- e^+ \nu$ and $K_S \to \pi^+ e^- \bar{\nu}$, respectively. The evaluated efficiencies for the different analysis steps are presented in Table 1.

Table 1. Efficiencies (%) for the different analysis steps.

Efficiency (%)	$K_S \to \pi^- e^+ \nu$	$K_S \to \pi^+ e^- \bar{\nu}$
trigger and event classification (ϵ_{TEC})	99.80 ± 0.02	99.80 ± 0.02
K_S tagging (ϵ_{TAG})	36.54 ± 0.05	36.67 ± 0.05
kinematical cuts (ϵ_{KC})	75.60 ± 0.07	75.62 ± 0.07
Track to Cluster Association (ϵ_{TCA})	42.22 ± 0.08	41.85 ± 0.08
Time of Flight (ϵ_{TOF})	64.03 ± 0.19	67.96 ± 0.18
Fit range (ϵ_{FR})	99.16 ± 0.03	99.17 ± 0.02

Using these efficiencies in eq. 3.1 the result for A_S is:

$$A_S = (-4.9 \pm 5.7_{stat}) \times 10^{-3}. \tag{5.4}$$

6 Systematic uncertainty

In order to estimate the contributions to the systematic uncertainty, the full analysis chain is repeated varying all the analysis cut values of selection variables by $+/-$ an amount comparable with their experimental resolution. The contributions from the stability of $M^2(e)$ distribution fit, momenta smearing, trigger and event classification procedures are also estimated. Unless differently specified in the following, each contribution is calculated as the absolute deviation from the nominal result (5.4) averaged on the two $+/-$ variations. The stability of the A_S result is also checked along the running period and against larger variations of the cut values.

The systematic uncertainties are classified into the following groups (see Table 2):

- Trigger and event classification:

  – Systematic effects originating from the trigger and the event classification procedure are estimated in prescaled data samples. The analysis of the prescaled samples follows the standard analysis chain. The systematic contribution (σ_{TEC}) is estimated to be 0.28×10^{-3}.

- Tagging and preselection:

  – The K_L deposited energy cut is changed to the values $E_{clu}(crash) = \{95, 105, 110, 115, 150, 200\}$ MeV. The stability of the result is checked within this range. The systematic uncertainty is evaluated by changing the cut by ± 5 MeV.

  – The β^* interval is enlarged or shrunk by 0.02 (1σ) on each side ($0.18 \mp 0.02 < \beta^* < 0.27 \pm 0.02$). The stability of the result is checked up to a variation of $\pm 5\sigma$.

  – The z_{vtx} and ρ_{vtx} cuts for the reconstructed $K_S \to \pi e \nu$ decay vertex position are each independently varied by ± 0.2 cm ($\pm 1\sigma$). The stability of the result is checked against a variation of $\pm 5\sigma$.

  – The range of the opening angle α of the charged secondaries in the K_S rest frame is enlarged or shrunk by $2°$ (1σ) on each side ($70 \mp 2° < \alpha < 175 \pm 2°$). The stability of the result is checked up to a variation of $\pm 5\sigma$ with the constraint of the upper bound not exceeding $180°$.

  – The $M_{inv}(\pi, \pi)$ interval is enlarged or shrunk by 1 MeV (1σ) on each side (300 ∓ 1 MeV $< M_{inv}(\pi, \pi) < 490 \pm 1$ MeV). The stability of the result is checked up to a variation of $\pm 5\sigma$.

- Time of flight selection:

  – The $|\delta_t(\pi, \pi)|$ cut is varied by ± 0.1 ns. The stability of the result is checked up to a variation of ± 0.4 ns.

  – The regions for the selection of the signal in the $\{\delta_t(e, \pi), \delta_t(\pi, e)\}$ plane are enlarged or shrunk by varying the cuts of ± 0.1 ns ($[|\delta_t(e, \pi)| < 1.3 \pm 0.1$ ns $, \delta_t(\pi, e) < -3.4 \pm 0.1$ ns] or $[\delta_t(e, \pi) > 3.4 \mp 0.1$ ns $, |\delta_t(\pi, e)| < 1.3 \pm 0.1$ ns]). The stability of the result is checked up to variations of ± 0.4 ns.

  – The circular region for selection of the signal in the $\{\delta_t(e), \delta_t(\pi)\}$ plane is enlarged or shrunk by varying its radius of ± 0.1 ns. The stability of the result is checked for variations ranging from -0.3 ns to $+0.4$ ns.

- Momenta smearing:

  – The $K_L \to \pi e \nu$ control sample is divided into ten, equal in luminosity subsamples. The momenta smearing parameters are tuned separately for each subsample. From the standard deviation of the results the systematic contribution (σ_{MS}) is estimated to be 0.58×10^{-3}.

- Fit procedure:

- The systematic uncertainty from the histogram bin width σ_{HBW} is determined by varying the bin width from 0.8 to 1.6 MeV^2/1000 (this variation corresponds to the $M^2(e)$ resolution evaluated from MC). σ_{HBW} is estimated to be 0.61×10^{-3}. The stability of the result is checked for variations of the bin width from 2σ to 5σ.
- The systematic uncertainty from the fit range is evaluated by varying it from $[-24 : 24]$ MeV^2/1000 to $[-28 : 28]$ MeV^2/1000 or $[-20 : 20]$ MeV^2/1000. The stability of the fit procedure is checked for histogram ranges from $[-36 : 36]$ MeV^2/1000 to $[-12 : 12]$) MeV^2/1000, while keeping the nominal bin size.

The total systematic uncertainty is estimated as the sum in quadrature of the contributions listed above and reported in Table 2.

As a cross-check, the A_L value for the $K_L \to \pi e \nu$ control sample is determined following the same analysis steps as for A_S. The result $A_L = (1.7 \pm 2.7_{stat}) \times 10^{-3}$ is consistent with the KTeV measurement [14].

Table 2. Summary of contributions to the systematic uncertainty on A_S.

Contribution		Systematic uncertainty (10^{-3})
Trigger and event classification	σ_{TEC}	0.28
Tagging and preselection	$E_{clu}(crash)$	0.55
"	β^*	0.67
"	z_{vtx}	0.01
"	ρ_{vtx}	0.05
"	α	0.46
"	$M_{inv}(\pi, \pi)$	0.20
Time of flight selection	$\delta_t(\pi, \pi)$	0.71
"	$\delta_t(e, \pi)$ vs $\delta_t(\pi, e)$	0.87
"	$\delta_t(e)$ vs $\delta_t(\pi)$	1.82
Momenta smearing	σ_{MS}	0.58
Fit procedure	σ_{HBW}	0.61
"	Fit range	0.49
Total		2.6

7 Results

The result for the $K_S \to \pi e \nu$ charge asymmetry is:

$$A_S = (-4.9 \pm 5.7_{stat} \pm 2.6_{syst}) \times 10^{-3}, \tag{7.1}$$

consistent with the previous determination on an independent data sample [17] and improving the statistical accuracy by almost a factor of two.

Taking into account the correlations of the systematical uncertainties of both measurements, based on similar analysis schemes, their combination provides:

$$A_S = (-3.8 \pm 5.0_{stat} \pm 2.6_{syst}) \times 10^{-3} \ . \tag{7.2}$$

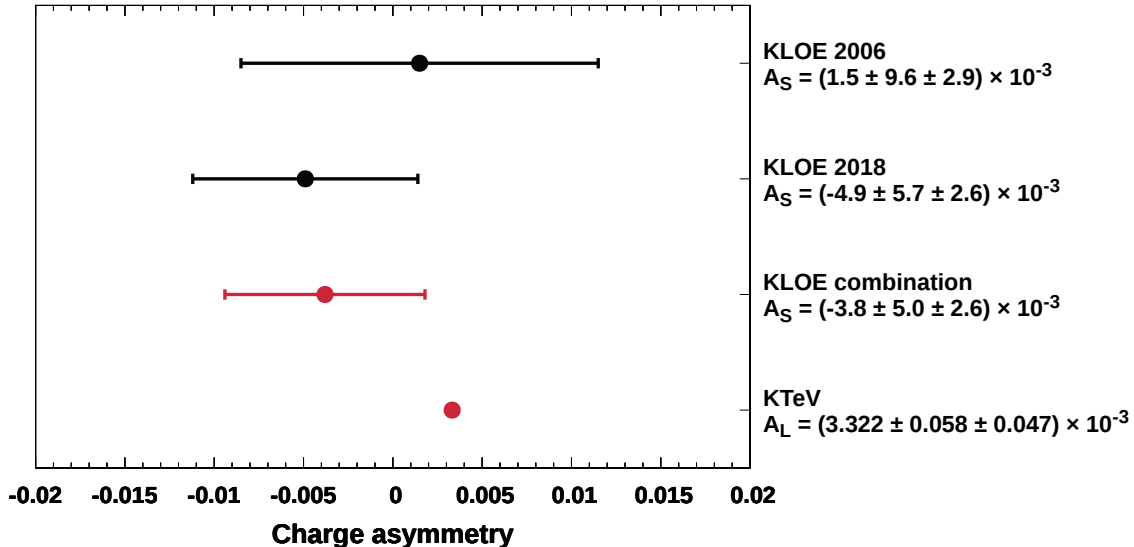A comparison of these results is shown in Figure 5.

Figure 5. Comparison of the previous result for A_S (KLOE 2006 [17]), the result presented in this paper (KLOE 2018) and the combination of the two. The KTeV result for A_L [14] is also shown. The uncertainties of the points correspond to the statistical and systematic uncertainties summed in quadrature.

The combined result 7.2 together with the KTeV result on A_L [14] yields for the sum and difference of asymmetries:

$$(A_S - A_L)/4 = Re(\delta_K) + Re(x_-) = (-1.8 \pm 1.4) \times 10^{-3}, \tag{7.3}$$

$$(A_S + A_L)/4 = Re(\epsilon_K) - Re(y) = (-0.1 \pm 1.4) \times 10^{-3}. \tag{7.4}$$

Using $Re(\delta_K) = (2.5 \pm 2.3) \times 10^{-4}$ [13] and $Re(\epsilon_K) = (1.596 \pm 0.013) \times 10^{-3}$ [12] the CPT violating parameters $Re(x_-)$ and $Re(y)$ are extracted:

$$Re(x_-) = (-2.0 \pm 1.4) \times 10^{-3}, \tag{7.5}$$

$$Re(y) = (1.7 \pm 1.4) \times 10^{-3}, \tag{7.6}$$

which are consistent with CPT invariance and improve by almost a factor of two the previous results [17].

Acknowledgments

References

[1] F. Niebergall et al., *Experimental study of the $\Delta S/\Delta Q$ rule in the time dependent rate of $K^0 \to \pi e \nu$*, *Phys. Lett. B* **49** (1974) 103.

[2] S. Bennett et al., *Measurement of the Charge Asymmetry in the Decay $K_L{}^0 \to \pi^\pm + e^\mp + \nu$*, *Phys. Rev. Lett.* **19** (1967) 993.

[3] KLOE collaboration, F. Ambrosino et al., *$|V_{us}|$ and lepton universality from kaon decays with the KLOE detector*, *JHEP* **4** (2008) 59.

[4] M. Antonelli et al., *An evaluation of $|V_{us}|$ and precise tests of the Standard Model from world data on leptonic and semileptonic kaon decays*, *Eur. Phys. J. C* **69** (2010) 399.

[5] M. Hayakawa and A. I. Sanda, *Searching for T, CP, CPT, and $\Delta S = \Delta Q$ rule violations in the neutral K meson system: A guide*, *Phys. Rev. D* **48** (1993) 1150.

[6] L. Maiani, *CP and CPT violation in neutral kaon decays*, in *The Second DAΦNE Physics Handbook* (L. Maiani, G. Pancheri, N. Paver, ed.), vol. I, p. 3. INFN-LNF, Frascati, 1995.

[7] G. Lüders, *Proof of the TCP Theorem*, *Ann. Phys.* **2** (1957) 1.

[8] N. E. Mavromatos, *Decoherence and CPT Violation in a Stringy Model of Space-Time Foam*, *Found. Phys.* **40** (2010) 917.

[9] S. Liberati, *Tests of Lorentz invariance: a 2013 update*, *Class. Quant. Grav.* **30** (2013) 133001.

[10] J. Bernabeu, A. Di Domenico and P. Villanueva-Perez, *Probing CPT in transitions with entangled neutral kaons*, *JHEP* **10** (2015) 139.

[11] J. S. Bell and J. Steinberger, *Weak interactions of kaons*, in *Proc. of the Oxford Int. Conf. on Elementary Particles*, 1965.

[12] KLOE collaboration, F. Ambrosino et al., *Determination of CP and CPT violation parameters in the neutral kaon system using the Bell-Steinberger relation and data from the KLOE experiment*, *JHEP* **12** (2006) 11.

[13] C. Patrignani, et al. (Particle Data Group), *Review of Particle Physics*, *Chin. Phys. C* **40** (2016) 100001.

[14] KTeV collaboration, A. Alavi-Harati et al., *Measurement of the K(L) Charge Asymmetry*, *Phys. Rev. Lett.* **88** (2002) 181601.

[15] A. Di Domenico, ed., *Handbook on Neutral Kaon Interferometry at a ϕ-factory*, vol. 43. Frascati Physics Series, 2007.

[16] A. Gallo et al., *DAFNE status report*, *Conf. Proc.* **C060626** (2006) 604.

[17] KLOE collaboration, F. Ambrosino et al., *Study of the branching ratio and charge asymmetry for the decay $K_S \to \pi e \nu$ with the KLOE detector, Phys. Lett. B* **636** (2006) 173.

[18] M. Adinolfi et al., *The Tracking detector of the KLOE experiment, Nucl. Instrum. Meth. A* **488** (2002) 51.

[19] M. Adinolfi et al., *The KLOE electromagnetic calorimeter, Nucl. Instrum. Meth. A* **482** (2002) 364.

[20] M. Adinolfi et al., *The trigger system of the KLOE experiment, Nucl. Instrum. Meth. A* **492** (2002) 134.

[21] F. Ambrosino et al., *Data handling, reconstruction, and simulation for the KLOE experiment, Nucl. Instrum. Meth. A* **534** (2004) 403.

[22] R. Barlow and C. Beeston, *Fitting using finite Monte Carlo samples, Computer Phys. Comm.* **77** (1993) 219.

[23] S. Baker and R. D. Cousins, *Clarification of the use of chi-square and likelihood functions in fits to histograms, Nucl. Instrum. Meth.* **221** (1984) 437.